Inorganic Chemistry

Article

pubs.acs.org/IC

# Unusual $Mn^{III/IV}_4$ Cubane and $Mn^{III}_{16}M_4$ (M = Ca, Sr) Looplike Clusters from the Use of Dimethylarsinic Acid

Nicole E. Chakov,[†] Annaliese E. Thuijs,[†] Wolfgang Wernsdorfer,[‡] Arnold L. Rheingold,[#] Khalil A. Abboud,[†] and George Christou*[,†]

[†]Department of Chemistry, University of Florida, Gainesville, Florida 32611-7200, United States

[‡]Laboratoire Louis Néel-CNRS, BP-166 Grenoble, Cedex 9, France

[#]Department of Chemistry, University of California at San Diego, La Jolla, California 92093-0358, United States

Supporting Information

**ABSTRACT:** Three complexes are reported from the initial use of dimethylarsinic acid ($Me_2AsO_2H$) in $Mn^{III/IV}$ cluster chemistry, $[Mn_4O_4(O_2AsMe_2)_6]$ (**3**; $2Mn^{III}$, $2Mn^{IV}$), and $[Mn_{16}X_4O_8(O_2CPh)_{16}(Me_2AsO_2)_{24}]$ (X = $Ca^{2+}$ (**4**) or $Sr^{2+}$ (**5**); $16Mn^{III}$). They were obtained from reactions with $[Mn_{12}O_{12}(O_2CR)_{16}(H_2O)_4]$ (R = Me, Ph) either without (**3**) or with (**4** and **5**) the addition of $X^{2+}$ salts. Complex **3** contains a $[Mn_4O_4]^{6+}$ cubane, whereas isostructural **4** and **5** contain a planar loop structure comprising four $Mn_4$ asymmetric "butterfly" units linked by alternating *anti,anti* $\mu$-$O_2AsMe_2$ and $\{X_2(O_2AsMe_2)(O_2CPh)_2\}$ units. Variable-temperature magnetic susceptibility ($\chi_M$) data were collected on dried microcrystalline samples of **3**−**5** in the 5.0−300 K range in a 0.1 T (1000 G) direct-current (dc) magnetic field. Data for **3** were fit to the appropriate Van Vleck equation (using the $\mathcal{H} = -2J\hat{S}_i\cdot\hat{S}_j$ convention) for a cubane of virtual $C_{2v}$ symmetry, giving $J_{33} = 0.0(1)$ cm$^{-1}$, $J_{34} = -3.4(4)$ cm$^{-1}$, $J_{44} = -9.8(2)$ cm$^{-1}$, and $g = 1.99(1)$, where the $J_{ij}$ subscripts refer to the oxidation states of the interacting Mn atoms. The ground state thus consists of two coupled $Mn^{IV}$ and two essentially noninteracting $Mn^{III}$. For **4** and **5**, low-lying excited states from the high nuclearity and weak couplings prevent fits of dc magnetization data, but in-phase alternating current susceptibility $\chi'_M T$ data down to 1.8 K indicate them to possess $S = 4$ ground states, if considered single $Mn_{16}$ units. If instead they are treated as tetramers of weakly coupled $Mn_4$ units, then each of the latter has an $S = 2$ ground state. Complexes **4** and **5** also exhibit very weak out-of-phase $\chi''_M$ signals characteristic of slow relaxation, and magnetization versus dc field scans on a single crystal of **4**·15MeCN at $T \geq 0.04$ K showed hysteresis loops but with unusual features suggesting the magnetization relaxation barrier consists of more than one contribution.

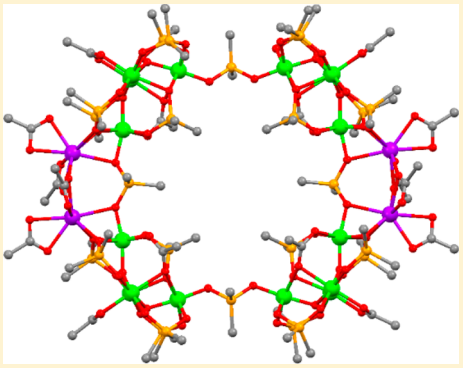

## INTRODUCTION

There continues to be great interest in the field of single-molecule magnets (SMMs) from groups around the world.[1,2] These are molecules that can function as molecular superparamagnets, and thus as magnets below their blocking temperature $T_B$. Although they only function as magnets at very low temperatures, SMMs nevertheless provide an alternative and very important "bottom-up" molecular approach to nanomagnetism, one that brings all the advantages of molecular chemistry to this field. Particularly crucial among the latter has been the crystallinity usually exhibited by molecular compounds, which provides a means for obtaining structural data at atomic resolution using single-crystal X-ray crystallography and for allowing detailed studies to be performed on highly ordered assemblies in the solid state by various spectroscopic and physical methods. The ready solubility of molecular species also allows the latter studies to be extended to characterization techniques common for the solution phase, including electrochemistry, multinuclear NMR spectroscopy, and others.

The field currently spans a wide range of metal types, from various d-metals to lanthanides and actinides[2−7] and combinations thereof,[8−11] as well as a whole spectrum of nuclearities, from mononuclear SMMs to giant ones such as $Mn_{70}$ and $Mn_{84}$ wheels of ∼4 nm diameter.[12] Among these, the prototypical SMM family, $[Mn_{12}O_{12}(O_2CR)_{16}(H_2O)_4]^z$, has been the most extensively studied, with its properties having been characterized as a function of carboxylate R group, oxidation level ($z$ = 0, 1, 2, 3),[13] local site-symmetry,[14] environmental influences,[15] and others, and has proven the major source to date of our knowledge on this nanomagnetic phenomenon.[2] Also widely explored has been the identity of the peripheral ligation, with carboxylates being very commonly employed, such as in the $Mn_{12}$ family, but also a wide variety of N- and/or O-based chelates.

Of relevance to the present work are the previous reports of ligand substitution of carboxylate groups in preformed clusters

**Received:** May 1, 2016
**Published:** August 9, 2016





DOI: 10.1021/acs.inorgchem.6b01077
*Inorg. Chem.* 2016, 55, 8468−8477

Table 1. Crystal Data and Structure Refinement Parameters for 3−5

| | 3·8$H_2O$ | 4·15MeCN | 5·16MeCN |
|---|---|---|---|
| formula[a] | $C_{12}H_{52}As_6Mn_4O_{24}$ | $C_{190}H_{269}Ca_4As_{24}Mn_{16}N_{15}O_{88}$ | $C_{192}H_{272}Sr_4As_{24}Mn_{16}N_{16}O_{88}$ |
| Fw, g $mol^{-1}$ | 1249.8 | 7008.6 | 7240.0 |
| space group | $P\bar{1}$ | $P2_1/c$ | $P2_1/c$ |
| $a$, Å | 11.7278(7) | 21.061(1) | 20.862(3) |
| $b$, Å | 13.7179(8) | 36.802(2) | 36.594(5) |
| $c$, Å | 14.0559(9) | 18.532(1) | 18.644(2) |
| $\alpha$, deg | 99.8690(10) | 90 | 90 |
| $\beta$, deg | 90.4520(10) | 94.3488(12) | 101.370(2) |
| $\gamma$, deg | 111.7540(1) | 90 | 90 |
| $V$, $Å^3$ | 2062.9(2) | 14 321.9 (16) | 13 953(3) |
| $Z$ | 2 | 2 | 2 |
| $T$, K | 218(2) | 100(2) | 100(2) |
| $\lambda$, Å[b] | 0.710 73 | 0.710 73 | 0.710 73 |
| $\rho_{calc}$, g/$cm^3$ | 1.983 | 1.625 | 1.725 |
| $R1$[c,d] | 0.0466 | 0.0876 | 0.0881 |
| $wR2$[e] | 0.1454 | 0.2286 | 0.2311 |

[a]Including solvent molecules. [b]Graphite monochromator. [c]$I > 2\sigma(I)$. [d]$R1 = 100\sum(||F_o| - |F_c||)/\sum|F_o|$. [e]$wR2 = 100[\sum[w(F_o^2 - F_c^2)^2]/\sum[w(F_o^2)^2]]^{1/2}$, $w = 1/[\sum^2(F_o^2) + [(ap)^2 + bp]$, where $p = [\max(F_o^2, O) + 2F_c^2]/3$.

not only with other carboxylic acids[2b,16] but also by other acids possessing an $XO_2^-$ unit that can bridge like a carboxylate, for example, in the common $\eta^1{:}\eta^1{:}\mu$ mode. Such "pseudocarboxylates" that have been used now span a range of different types, namely, with X = N, P, S, and Se. For example, ligand substitution reactions on the $Mn_{12}$ family were first reported using 4 equiv of nitric acid, which site-specifically converted $[Mn_{12}O_{12}(O_2CR)_{16}(H_2O)_4]$ to $[Mn_{12}O_{12}(O_2CR)_{12}(NO_3)_4(H_2O)_4]$.[17] Similarly, reactions of diphenylphosphinic acid ($Ph_2PO_2H$) (8:1 ratio) or diphenylphosphoric acid ($(PhO)_2PO_2H$) (4:1) with $[Mn_{12}O_{12}(O_2CR)_{16}(H_2O)_4]$ gave $[Mn_{12}O_{12}(O_2CR)_{16-n}(O_2PPh_2)_n(H_2O)_4]$ ($n$ = 8, 9)[18] and $[Mn_{12}O_{12}(O_2CR)_{12}(O_2P(OPh)_2)_4]$,[19] respectively. Benzenesulfonic acid ($PhSO_3H$) possesses three O atoms but again behaves as a pseudocarboxylic acid in an 8:1 reaction with $Mn_{12}$ to give $[Mn_{12}O_{12}(O_2CR)_8(O_2SOPh)_8(H_2O)_4]$.[20] The smaller methanesulfonic acid, however, leads to $\mu_3$-$O_3SMe$ bridging groups.[21] In all these cases, the $[Mn_{12}O_{12}]^{16+}$ core was essentially unaffected, the substitution causing only a small distortion. In contrast, the reaction of $Mn_{12}$ with an excess (18:1) of benzeneseleninic acid ($PhSeO_2H$) causes core rupture and the formation of extremely interesting $[Mn_7O_8(O_2SePh)_{9-n}(O_2CMe)_n(H_2O)]$ ($n$ = 0, 1; $3Mn^{III}$, $4Mn^{IV}$) products of unprecedented structure, one of which was found to be a single-chain magnet (SCM).[22] Note that $PhSeO_2^-$ is similar to $RCO_2^-$ and $NO_3^-$ in having a three-coordinate central atom (unlike $Ph_2PO_2^-$ and $RSO_3^-$) but different in also having a stereochemically active lone pair.

As part of a continuing interest in the use of noncarboxylate ligands in $Mn_{12}$ chemistry, we decided to explore an acid further down group 15, analogous to Se in group 16, and chose dimethylarsinic acid ($Me_2AsO_2H$). This is similar to $Ph_2PO_2H$, and a survey of the literature showed that in Mo chemistry $Me_2AsO_2^-$ analogues of $Ph_2PO_2^-$ complexes can be prepared.[23] We herein report the syntheses, X-ray structures, and magnetic properties of a homometallic $Mn_4O_4$ cubane and two heterometallic $Mn_{16}M_4$ (M = Ca, Sr) looplike clusters from the use of $Me_2AsO_2H$ with $Mn_{12}$.

## EXPERIMENTAL SECTION

**Synthesis.** All manipulations were performed under aerobic conditions using materials as received (Sigma-Aldrich), except where noted otherwise. $[Mn_{12}O_{12}(O_2CMe)_{16}(H_2O)_4]\cdot 2MeCO_2H\cdot 4H_2O$ (**1**) and $[Mn_{12}O_{12}(O_2CPh)_{16}(H_2O)_4]$ (**2**) were prepared as described elsewhere.[2a,24]

*$[Mn_4O_4(O_2AsMe_2)_6]$ (**3**).* A solution of complex **1** (0.50 g, 0.24 mmol) in MeCN (75 mL) was treated with $Me_2AsO_2H$ (0.60 g, 4.3 mmol) in MeCN (25 mL) and stirred overnight. The solvent was removed from the resulting deep red solution by rotoevaporation under vacuum, the residue was treated with toluene (25 mL), and the solution was again evaporated to dryness. The addition and removal of toluene was repeated three more times. The residue was then dissolved in $CH_2Cl_2$ (50 mL), filtered through diatomaceous earth, and carefully layered with pentane. Large dark red crystals of **3**·8$H_2O$ slowly formed over 6 d. The sample for X-ray crystallography was maintained in mother liquor to prevent loss of interstitial solvent. Otherwise, the crystals were isolated by filtration, washed copiously with pentane, and dried in vacuo; the yield was 0.20 g (75%). Anal. Calcd (found) for **3**·$H_2O$ ($C_{12}H_{38}As_6Mn_4O_{17}$): C, 12.83 (12.79); H, 3.41 (3.48); N, 0.00 (0.00)%. Selected IR data (KBr disk, $cm^{-1}$): 3420 (b), 3016 (m), 2965 (m), 2926 (m), 2878 (m), 1653 (w), 1568 (s), 1473 (w), 1420 (s), 1272 (m), 1094 (s), 808 (vs), 652 (m), 622 (s), 565 (m), 500 (s), 481 (s).

*$[Mn_{16}Ca_4O_8(O_2CPh)_{16}(O_2AsMe_2)_{24}]$ (**4**).* A stirred slurry of complex **2** (0.25 g, 0.087 mmol) in MeCN (10 mL) was treated with solid $Me_2AsO_2H$ (0.22 g, 1.6 mmol) and solid $Ca(NO_3)_2\cdot 4H_2O$ (0.021 g, 0.087 mmol), and MeOH (1 mL) was added to aid solubility. Stirring was continued for 20 min, and the resulting dark red solution was filtered through diatomaceous earth to remove some fine brown powder. The filtrate was layered with $Et_2O$, and dark red crystals of **4**·15MeCN slowly formed over 3 d. The crystallographic sample was maintained in mother liquor; otherwise, the crystals were collected by filtration, washed with MeCN, and dried under vacuum. The yield was 0.03 g (5%). Anal. Calcd (found) for **4**·2MeCN ($C_{164}H_{230}N_2As_{24}Ca_4O_{88}Mn_{16}$): C, 30.42 (30.04); H, 3.58 (3.44); N, 0.43 (0.46)%. Selected IR data ($cm^{-1}$): 3422 (b), 3016 (w), 2924 (w), 2268 (s), 1597 (m), 1550 (m), 1394 (s), 1269 (w), 799 (vs), 721 (m), 649 (m), 588 (m), 484 (s).

*$[Mn_{16}Sr_4O_8(O_2CPh)_{16}(O_2AsMe_2)_{24}]$ (**5**).* The synthesis was performed as for complex **5** except that $Sr(ClO_4)_2\cdot H_2O$ (0.025 g, 0.087 mmol) was used instead of $Ca(NO_3)_2\cdot 4H_2O$, and the dark red crystals of **5**·16MeCN were collected after 5 d; the yield was 0.04 g (7%). Anal. Calcd (found) for solvent-free **5** ($C_{160}H_{224}As_{24}Sr_4O_{88}Mn_{16}$): C, 29.19 (29.42); H, 3.43 (3.66); N, 0.00 (0.00)%. Selected IR data ($cm^{-1}$):


DOI: 10.1021/acs.inorgchem.6b01077
Inorg. Chem. 2016, 55, 8468−8477

3421 (m,br), 2930 (w), 1597 (s), 1550 (s), 1394 (vs), 1268 (w), 1023 (w), 833 (vs), 800 (vs), 720 (m), 675 (m), 667 (w), 651 (m), 613 (w), 592 (w), 490 (m), 459 (w), 447 (w), 416 (w).

**X-ray Crystallography.** Data were collected on a Bruker P4 (**3**·$8H_2O$) or Siemens SMART PLATFORM (**5**·16MeCN) platform goniometer equipped with a SMART APEX CCD area detector and on a Bruker DUO diffractometer (**4**·15MeCN) with an APEXII CCD area detector. Suitable single crystals were attached to glass fibers using silicone grease and transferred to the goniostat, where they were cooled for characterization and data collection. The structures were solved by direct methods (SHELXTL)[25] and standard Fourier techniques, and they were refined on $F^2$ using full-matrix least-squares cycles. All non-H atoms (except some disordered C atoms) were refined anisotropically, whereas H atoms were placed in calculated positions and refined isotropically using a riding model. Cell parameters were refined using 8192 reflections. The intensity data for **3**·$8H_2O$ were collected using the $\varphi$-scan method with a scan step $\Delta\varphi = 0.03°$. For **4**·15MeCN, raw data frames were read by program SAINT and integrated using three-dimensional profiling algorithms. The resulting data were reduced to produce *hkl* reflections and their intensities and estimated standard deviations. For **5**·16MeCN, a full sphere of data (1850 frames) was collected using the $\omega$-scan method (0.3° frame width). The first 50 frames were remeasured at the end of data collection to monitor instrument and crystal stability (maximum correction on $I$ was <1%). Data for **3**·$H_2O$ were corrected for Lorentz and polarization effects using the Bruker SAINT software,[25b] and an absorption correction was performed using the SADABS program[25c] supplied by Bruker AXS ($T_{min}/T_{max} = 0.657$). Absorption corrections by integration were applied for **4**·15MeCN and **5**·16MeCN based on measured indexed crystal faces. Crystal data and structure refinement parameters are listed in Table 1.

For **3**·$8H_2O$, the asymmetric unit contains the $Mn_4$ cluster and eight water molecules of crystallization. Seven of the latter were observed and refined, but one was too disordered to be modeled properly, and the program SQUEEZE,[26] part of the PLATON[27] package of crystallographic software, was therefore used to calculate the solvent disorder area and remove its contribution to the overall intensity data. There were 457 parameters in the final cycle of refinement using 8006 independent reflections with $I > 2\sigma(I)$ to yield $R1$ and $wR2$ of 3.70 and 14.54%, respectively. The final difference Fourier map was reasonably clean, the largest electron density peak and deepest hole being 3.23 and −1.07 e/Å$^3$, respectively; they were located within 1 Å of the heavy elements (Mn and As), and thus were attributed to their anisotropy.

For **4**·15MeCN, the asymmetric unit contains one-half of a $Mn_{16}$ molecule on an inversion center and 7.5 MeCN molecules. The latter were disordered, and SQUEEZE was again used to remove their contribution. Three benzoate Ph rings [C32−C37, C72−C77, C92−C97] were rotationally disordered and refined as rigid bodies. The $AsMe_2$ atoms of two $Me_2AsO_2^-$ ligands [As6, C11, C12 and As9, C17, C18] were disordered and resolved; their site occupancies were fixed at 50%. There were 380 parameters in the final cycle of refinement using 26 952 reflections with $I > 2\sigma(I)$ to yield $R1$ and $wR2$ of 8.76 and 22.86%, respectively. The final difference Fourier map was reasonably clean, the largest peak and deepest hole being 1.50 and −1.45 e/Å$^3$, respectively, located within 1 Å of the heavy elements.

For **5**·16MeCN, the asymmetric unit contains one-half of a $Mn_{16}$ molecule on an inversion center and eight MeCN molecules. The latter were disordered, and SQUEEZE was again used to remove their contribution. Three benzoate Ph rings [on C31, C51, and C91] were disordered and were dependently refined as rigid bodies (AFIX 66). Other Ph rings were either not disordered or the disorder was minor and could not be resolved, and all were also refined as rigid bodies. The $AsMe_2$ atoms of four $Me_2AsO_2^-$ ligands were disordered about two (main) positions [As4/As4′, As10/As11, As12/As13, As14/As15] whose occupation factors were fixed in the last refinement cycles. There were 1096 parameters in the final refinement cycle using 10 406 reflections with $I > 2\sigma(I)$ to yield $R1$ and $wR2$ of 8.81 and 23.11%, respectively. The final difference Fourier map was reasonably clean, the largest peak and deepest hole being 3.4 (representing traces of a disordered As) and −1.1 e/Å$^3$, respectively, located within 1 Å of the heavy elements.

**Other Studies.** Infrared spectra were recorded in the solid state (KBr pellets) on a Nicolet Nexus 670 FTIR spectrometer in the 400−4000 cm$^{-1}$ range. Elemental analyses (C, H, and N) were performed by the in-house facilities of the University of Florida Chemistry Department. Variable-temperature direct-current (dc) and alternating-current (ac) magnetic susceptibility data were collected on vacuum-dried solids using a Quantum Design MPMS-XL SQUID magnetometer equipped with a 7 T magnet and operating in the 1.8−300 K range. Samples were embedded in solid eicosane in a gel capsule to prevent torquing. Diamagnetic and background contributions from the eicosane and gel capsule were measured as a blank and subtracted from the susceptibility. Magnetization versus field and temperature data were fit using the program MAGNET.[28] Pascal's constants[29] were used to estimate the diamagnetic correction, which was subtracted from the experimental susceptibility to give the molar paramagnetic susceptibility ($\chi_M$).

## RESULTS AND DISCUSSION

**Syntheses.** As described in the Introduction, reactions of $Mn_{12}$ with 4 or 8 equiv of $Ph_2PO_2H$, $(PhO)_2PO_2H$, $PhSO_3H$, $MeSO_3H$, and $HNO_3$ gave modified $Mn_{12}$ SMMs products, while an 18:1 excess of $PhSeO_2H$ transformed the $Mn_{12}$ into an interesting new $Mn_7$ structural type. In the present work, we thus explored the analogous 18:1 reaction in MeCN of **1** with $Me_2AsO_2H$. This caused a rapid color change from a dark brown to a deep red solution, from which was subsequently isolated $[Mn_4O_4(O_2AsMe_2)_6]$ (**3**; $2Mn^{III}$, $2Mn^{IV}$) in ∼75% yield as **3**·$8H_2O$. Multiple cycles of acetic acid removal as its toluene azeotrope were considered important for complete substitution, because $Me_2AsO_2H$ ($pK_a = 6.27$)[30] is significantly less acidic than $MeCO_2H$ ($pK_a$= 4.76). The structure of **3** (vide infra) is analogous to that of $[Mn_4O_4(O_2PPh_2)_6]$ obtained from the reaction of $[Mn_{12}O_{12}(O_2CMe)_8(O_3SPh)_8(H_2O)_4]$ with $Ph_2PO_2H$,[20b] suggesting that such reactions with $Mn_{12}$ might be a convenient general route to $[Mn_4O_4]^{6+}$ cubane complexes. $Me_2AsO_2H$ and $PhSeO_2H$ thus give different structural types from an 18:1 reaction with **1**, $Mn_4$ versus $Mn_7$, respectively, but interestingly both give high oxidation state $Mn^{III}/Mn^{IV}$ products. Attempts to back-replace some or all of the $Me_2AsO_2^-$ groups on preformed **3** with $RCO_2^-$ groups by treatment with $RCO_2H$ (R = Me, Et, $Cl_2CH$, $^tBuCH_2$) to access unknown $[Mn_4O_4(O_2CR)_6]$ complexes were unsuccessful, as judged by IR spectra of isolated solids.

We extended the use of $Me_2AsO_2H$ in several directions, and one of them is heterometallic chemistry that has yielded interesting Mn/Ca and Mn/Sr products. Initial reactions of **3** with various $Ca^{2+}$ salts such as $Ca(NO_3)_2$, $Ca(O_2CMe)_2$, and $Ca(ClO_4)_2$ were unsuccessful, leading only to isolation of unreacted **3**, so we instead added $Ca^{2+}$ salts to the preparative reaction to **3**. However, we could not isolate any Mn/Ca products from these reactions, but use of the benzoate analogue **2** proved successful. Thus, **2** was treated with $Ca(NO_3)_2$ and $Me_2AsO_2H$ in a 1:1:18 ratio in MeCN/MeOH. The solution changed from dark brown to dark red within 20 min, and from it was subsequently isolated well-formed dark red crystals of $[Mn_{16}Ca_4O_8(O_2CPh)_{16}(Me_2AsO_2)_{24}]$ (**4**) as **4**·15MeCN. The same reaction but with $Sr(ClO_4)_2$ instead of $Ca(NO_3)_2$ proceeded analogously and gave $[Mn_{16}Sr_4O_8(O_2CPh)_{16}(Me_2AsO_2)_{24}]$ (**5**) as **5**·16MeCN. The yields of both complexes are very low, 5 and 7%, respectively, but the syntheses are fully reproducible. Given the stability of **3**, as reflected in its inertness to reactions with $RCO_2H$ or $Ca^{2+}$ salts, we suspect


DOI: 10.1021/acs.inorgchem.6b01077
Inorg. Chem. 2016, 55, 8468−8477

that it is a major side-product in the syntheses of **4** and **5**, and we were perhaps very fortunate to have been able to isolate any pure **4** and **5**; the typically lower solubility of benzoate compounds in highly polar solvents such as MeCN and MeOH was probably a factor in the preferential crystallization of **4** and **5** and probably also rationalizes why the use of **1** did not give their acetate analogues. We explored whether we could isolate additional material from the filtrates to obtain more **4** and **5** and/or confirm **3** as a significant product of the reaction, but we could not isolate any pure material, only sticky solids suggestive of mixtures. We also explored the use of EtOH instead of MeOH, but the same products were obtained in comparable yield; omission of any alcohol gave powder precipitates we could not characterize. Overall, we were thus happy to settle for small yields of pure, highly crystalline **4** and **5**.

**Description of Structures.** The structure of **3** and a stereoview are shown in Figure 1, and selected distances and

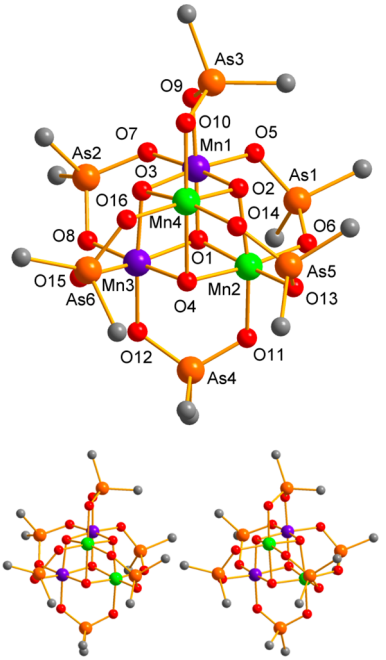


**Figure 1.** (top) Partially labeled structure of **3** and (bottom) a stereopair. Color code: $Mn^{III}$ green, $Mn^{IV}$ blue, As orange, O red, C gray. H atoms were omitted for clarity.

angles are listed in Table S1.[31] The structure consists of a $[Mn^{III}_2Mn^{IV}_2(\mu_3\text{-}O)_4]^{6+}$ core with the peripheral ligation provided by six syn,syn $\eta^1{:}\eta^1{:}\mu$ $Me_2AsO_2^-$ groups. The complex has crystallographic $C_1$ and virtual $C_{2v}$ symmetry, with the $C_2$ axis passing through the midpoints of the $Mn^{III}$–$Mn^{III}$ and $Mn^{IV}$–$Mn^{IV}$ vectors. Core metric parameter ranges under $C_{2v}$ are collected in Table 2.

The Mn oxidation states and central $\mu_3$-O protonation levels were deduced from charge considerations and the Mn–O bond distances and were confirmed by bond valence sum (BVS) calculations (Table 3),[32] indicating that Mn1 and Mn3 are $Mn^{IV}$, Mn2 and Mn4 are $Mn^{III}$, and that $\mu_3$-$O^{2-}$ ions are bridging in the cubic core. All the Mn are six-coordinate with near-octahedral geometry, and the two $Mn^{III}$ atoms display Jahn–Teller (JT) elongations, as expected,[33] along the O2–Mn2–O11 and O4–Mn4–O10 axes, which are parallel and both equatorial relative to the virtual $C_2$ axis. The JT elongated

**Table 2. Summary of Core Bond Distances (Å) and Angles (deg) for 3**

| parameter[a,b] | range |
|---|---|
| $Mn^{IV}$–$O_c$ (ax) | 1.840(4), 1.856(4) |
| $Mn^{IV}$–$O_c$ (eq) | 1.875(4)–1.959(4) |
| $Mn^{III}$–$O_c$ (ax) | 1.935(4), 1.970(4) |
| $Mn^{III}$–$O_c$ (eq) | 1.893(4)–2.288(4) |
| $Mn^{IV}$–$O_{eq}$ | 1.909(4)–1.959(4) |
| $Mn^{IV}$–$O_{ax}$ | 1.934(4), 1.940(4) |
| $Mn^{III}$–$O_{eq}$ | 1.922(4)–2.094(4) |
| $Mn^{III}$–$O_{ax}$ | 1.904(4), 1.931(4) |
| $Mn^{IV}\cdots Mn^{IV}$ | 2.885(1) |
| $Mn^{III}\cdots Mn^{III}$ | 3.054(1) |
| $Mn^{IV}\cdots Mn^{III}$ | 2.863(1)–3.016(1) |
| $Mn^{IV}$–$O_c$-$Mn^{IV}$ | 97.18(17), 97.62(17) |
| $Mn^{III}$–$O_c$-$Mn^{III}$ | 93.35(16), 98.02(17) |
| $Mn^{III}$–$O_c$-$Mn^{IV}$ | 93.26(16)–100.27(17) |

[a]Collected under $C_{2v}$ virtual symmetry. [b]$O_c$ = cubane $O^{2-}$, $O_{ax}$ = axial arsinate, $O_{eq}$ = equatorial arsinate. [c]eq/eq $O^{2-}$ angles. [d]ax/eq $O^{2-}$ angles.

**Table 3. Bond Valence Sum and Assignments for Mn and O Atoms in 3–5**

| | atom[a] | $Mn^{II}$ | $Mn^{III}$ | $Mn^{IV}$ | atom[b] | BVS | ion |
|---|---|---|---|---|---|---|---|
| **3** | Mn1 | 4.17 | 3.82 | **4.01** | O1 | 1.93 | $O^{2-}$ |
| | Mn2 | 3.47 | **3.18** | 3.34 | O2 | 1.82 | $O^{2-}$ |
| | Mn3 | 3.85 | 3.52 | **3.70** | O3 | 1.90 | $O^{2-}$ |
| | Mn4 | 3.18 | **2.91** | 3.06 | O4 | 1.75 | $O^{2-}$ |
| **4** | Mn1 | 3.15 | **2.89** | 3.03 | O1 | 2.05 | $O^{2-}$ |
| | Mn2 | 3.33 | **3.04** | 3.20 | O2 | 1.99 | $O^{2-}$ |
| | Mn3 | 3.24 | **2.96** | 3.11 | O3 | 2.01 | $O^{2-}$ |
| | Mn4 | 3.17 | **2.90** | 3.05 | O4 | 1.98 | $O^{2-}$ |
| | Mn5 | 3.17 | **2.90** | 3.04 | | | |
| | Mn6 | 3.21 | **2.94** | 3.09 | | | |
| | Mn7 | 3.24 | **2.96** | 3.11 | | | |
| | Mn8 | 3.21 | **2.94** | 3.08 | | | |
| **5** | Mn1 | 3.12 | **2.85** | 3.00 | O5 | 2.05 | $O^{2-}$ |
| | Mn2 | 3.21 | **2.93** | 3.08 | O6 | 2.05 | $O^{2-}$ |
| | Mn3 | 3.24 | **2.97** | 3.12 | O33 | 2.04 | $O^{2-}$ |
| | Mn4 | 3.18 | **2.91** | 3.05 | O34 | 2.03 | $O^{2-}$ |
| | Mn5 | 3.01 | **2.75** | 2.89 | | | |
| | Mn6 | 3.21 | **2.94** | 3.09 | | | |
| | Mn7 | 3.23 | **2.96** | 3.10 | | | |
| | Mn8 | 3.04 | **2.78** | 2.92 | | | |

[a]The bold value is the one closest to the charge for which it was calculated. The oxidation state is the nearest integer to the bold value. [b]An O BVS in the ~1.8–2.0, ~1.0–1.2, and ~0.2–0.4 ranges indicates non, single, and double protonation, respectively.

and equatorial $Mn^{III}$–O are 2.066(3)–2.290(3) Å and 1.893(3)–1.974(3) Å, respectively. The $Mn^{IV}$ atoms, Mn1 and Mn3, exhibit shorter Mn–O bond lengths in the range of 1.838(3)–1.959(3) Å and lack JT elongation axes, showing that the complex is trapped-valence and crystallographically ordered. The $Mn^{III}$ JT elongation axes normally avoid Mn-oxide bonds, almost always the strongest and shortest in the molecule, but in a $\{Mn_4O_4\}$ cubane this is not possible; thus, $Mn^{III}$–$O^{2-}$ bonds Mn2–O2 and Mn4–O4 are JT elongated to 2.290(3) and 2.139(3) Å, respectively (the non-JT Mn2–O4 and Mn4–O2 are 1.897(3) and 1.899(3)Å, respectively). As a result the cubane core is distinctly distorted. It is noteworthy that the JT-elongated $Mn^{III}$–$O^{2-}$ bonds are remarkably long, even longer



DOI: 10.1021/acs.inorgchem.6b01077
Inorg. Chem. 2016, 55, 8468–8477

**Table 4. Ligand O···O Distances (Å) in Carboxylate and Pseudocarboxylate Groups**

| acid | compound | O···O[a] | p$K_a$[52−55] | ref |
|---|---|---|---|---|
| $MeCO_2H$ | $[Mn_{12}O_{12}(O_2CMe)_{16}(H_2O)_4]$ | 2.235−2.249 | 4.76 | 24 |
| $PhSO_3H$ | $[Mn_{12}O_{12}(O_2CMe)_8(O_3SPh)_8(H_2O)_4]$ | 2.400−2.422[b] | 2.55 | 20 |
| $Ph_2PO_2H$ | $[Mn_{12}O_{12}(O_2CMe)_8(O_2PPh_2)_8(H_2O)_4]$ | 2.561−2.565[b] | 2.32 | 14 |
| | $[Mn_4O_4(O_2PPh_2)_6]$ | 2.566−2.617 | | 18 |
| $PhSeO_2H$ | $[Mn_7O_8(O_2CMe)(O_2SePh)_8(H_2O)]$ | 2.654−2.799[b] | 4.79 | 22 |
| | $[Mn_7O_8(O_2SePh)_9(H_2O)]$ | 2.640−2.836 | | 22 |
| $Me_2AsO_2H$ | $[Mn_4O_4(O_2AsMe_2)_6]$ | 2.797−2.834 | 6.27 | this work |

[a]The O···O distance of the bound O atoms. [b]For the noncarboxylate groups.

than the JT-elongated Mn−O(arsinate) bonds trans to them (Mn2−O11 = 2.066(3), Mn4−O10 = 2.096(3) Å). Compare this with the JT elongation axis of the fast-relaxing $Mn_{12}$ clusters, where the Mn−$O^{2-}$ bond is 2.073(7) Å and the *trans*-Mn−O(carboxylate) is 2.160(8) Å.[34] This suggests the Mn−O(arsinate) bond is more difficult to elongate than the Mn−$O^{2-}$ bond either due to the limited flexibility of the $Me_2AsO_2^-$ group or, more likely, a significantly greater Mn−O(arsinate) versus Mn−O(carboxylate) bond strength due to greater electron density at the O atoms, as also reflected in the high p$K_a$ of $Me_2AsO_2H$ of 6.27. As expected, the lattice water molecules form hydrogen bonds to other water molecules (O···O distances in the 2.7−2.9 Å range) and to O atoms of $Me_2AsO_2^-$ groups (O···O in the 2.8−3.0 Å range) giving two-dimensional H-bonded sheets with no H bonds between them.

There are a number of reported examples of $Me_2AsO_2^-$ bridging Fe,[35] Zn,[36] Zr,[37] Mo,[38,39] and W[39d] in the pseudocarboxylate manner seen in **3**, but the latter is the first example to our knowledge of the use of $Me_2AsO_2^-$ in Mn chemistry. However, a $Mn_8$ complex was recently reported using $PhAsO_3H$ and dipicolinic acid.[40] In addition, several other complexes with the discrete $\{Mn_4(\mu_3\text{-}O)_4\}$ cubane core have been reported, namely, $[Mn^{III}_2Mn^{IV}_2O_4(O_2PR_2)_6]$ (R = Ph or $OC_6H_4$-*p*-Me)[41] at the same oxidation level as **3**, $[Mn^{III}Mn^{IV}_3O_4(O_2PPh_2)_6]$[42] and $[Mn^{III}_4O_2(OMe)_2(HOMe)(O_2P(OC_6H_4\text{-}p\text{-}Me)_2)_6]$[41b] from Dismukes and co-workers, and the $[Mn^{III}_3Mn^{IV}O_3(\mu_3\text{-}X)]^{6+}$ (X = $Cl^-$, $F^-$, $Br^-$, $N_3^-$, $NCO^-$, $RCO_2^-$, etc.) family from our own group.[43,44]

In Table 4 are compared a few pertinent properties of some pseudocarboxylate groups used to date in Mn chemistry, particularly their basicities and the O···O distances of bound O atoms in the syn,syn $\eta^1$:$\eta^1$:$\mu$ mode. The various ligands have not been explored extensively or under identical conditions, so we avoid firm conclusions, but some a posteriori comments are appropriate: (i) $PhSO_3^-$ and $Ph_2PO_2^-$, the less basic, weaker donor ligands in the table, as reflected by the p$K_a$ of their conjugate acids, are the only ones (to date) to be able to substitute carboxylates of $[Mn_{12}O_{12}(O_2CMe)_{16}(H_2O)_4]$ without core transformation; (ii) these ligands also exhibit O···O distances only ∼0.2−0.3 Å greater than carboxylates, primarily due to the longer P−O and S−O bonds; (iii) $PhSeO_2^-$ and $Me_2AsO_2^-$, the more basic, stronger donor ligands, and with O···O distances ≥0.4 Å longer than carboxylates, have all given $Mn_{12}$ rupture and new product core topologies; and (iv) it is interesting that only $Ph_2PO_2^-$ and $Me_2AsO_2^-$ have yielded a $[Mn_4O_4(O_2XR_2)_6]$ cubane to date, even though the basicities are so different due to both the more electronegative P versus As and the electron-withdrawing Ph substituents, suggesting that the tetrahedral nature of the X atom is important in stabilizing the cubane. Since $PhSeO_2^-$ has a stereochemically active lone pair and O···O distances comparable with $Me_2AsO_2^-$, the one speculative prediction we will venture is that $[Mn_4O_4(O_2SePh)_6]$ is likely capable of synthesis.

Two views of the structure of **4** and a stereoview are shown in Figure 2. The structure of **5** is essentially superimposable (Figure S1)[45] and is not shown or described separately; selected interatomic distances and angles for **4** and **5** are

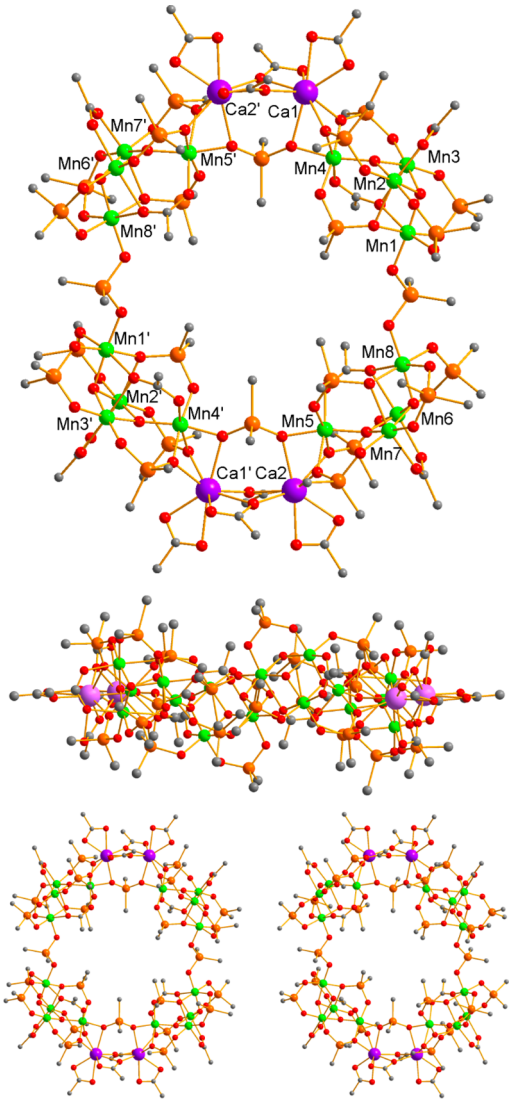


**Figure 2.** (top) Top-view of the structure of centrosymmetric **4**, (middle) a side-view emphasizing its planarity, and (bottom) a stereopair. For clarity, H atoms were omitted, and only the ipso C atoms of the benzoate Ph rings are shown. Color code: $Mn^{III}$ green, Ca violet, As orange, O red, C gray.



DOI: 10.1021/acs.inorgchem.6b01077
*Inorg. Chem.* 2016, 55, 8468−8477

compared in Table 5. The complexes crystallize in monoclinic space group $P2_1/c$, with the molecules lying on crystallographic

**Table 5. Comparison of Selected Distances (Å) and Angles (deg) for 4 and 5**

| parameter[a] | 4 (X = Ca) | 5 (X = Sr) |
|---|---|---|
| $Mn_w$–$O_{ox}$ | 1.872(4)–1.886(4) | 1.867(10)–1.908(9) |
| $Mn_b$–$O_{ox}$ | 1.890(4)–1.920(4) | 1.880(11)–1.925(10) |
| $Mn_b\cdots Mn_w$[b] | 3.388(2)–3.447(2) | 3.378(3)–3.442(4) |
| $Mn_b\cdots Mn_w$[c] | 3.048(2)–3.147(2) | 3.081(3)–3.160(3) |
| $Mn_b\cdots Mn_b$ | 2.818(2), 2.826(2) | 2.821(3), 2.823(3) |
| $X^{2+}\cdots X^{2+}$ | 3.825(2) | 4.017(2) |
| $X^{2+}\cdots Mn_w$ | 3.220(2), 3.223(2) | 3.370(3), 3.377(3) |
| $O_{ox}\cdots Mn_b\cdots O_{ox}$ | 82.05(16)–83.09(16) | 81.5(4)–82.7(5) |
| $Mn_b\cdots O_{ox}\cdots Mn_b$ | 94.76(16)–95.64(16) | 95.1(4)–96.0(5) |
| $Mn_w\cdots O_{ox}\cdots Mn_b$[b] | 127.1(2)–130.5(2) | 126.2(5)–131.4(5) |
| $Mn_w\cdots O_{ox}\cdots Mn_b$[c] | 106.7(2)–112.5(2) | 108.2(5)–114.2(5) |

[a]w = wingtip, b = body, $O_{ox}$ = $\mu_3$-oxide. [b]Singly monoatomically bridged. [c]Doubly monoatomically bridged.

inversion centers; for brevity, references to specific atoms in the following discussion implicitly include their symmetry-related partners. The structure consists of four $[Mn^{III}_4(\mu_3\text{-}O)_2(\mu\text{-}OR)_2]$ asymmetric "butterfly" units (R is the rest of a $PhCO_2^-$ or $Me_2AsO_2^-$ group) linked together into a loop by alternating *anti,anti* $\mu$-$O_2AsMe_2$ and $\{Ca_2(O_2AsMe_2)(O_2CPh)_2\}$ units attached at the $Mn_w$ (w = wingtip) atoms. Peripheral ligation is completed by additional $Me_2AsO_2^-$ and $PhCO_2^-$ groups in various binding modes (vide infra). The side view (Figure 2, middle) emphasizes the planarity of the molecule. The Ca are eight-coordinate with Ca–O bonds in the 2.33–2.61 Å range. $Mn^{III}$ oxidation states and $O^{2-}$ protonation levels were again confirmed by BVS calculations (Table 3).[32] All $Mn^{III}$ are nearly octahedral and exhibit clear JT axial elongation of two trans bonds; as expected, the JT axes avoid $Mn^{III}$–$O^{2-}$ bonds. The four JT axes of $Mn_b$ (b = body) atoms Mn(2,2′,3,3′) are essentially parallel, as are those of body Mn(6,6′,7,7′), and the two sets are at an angle of 61° to each other and both in the plane of the molecule. The JT axes at wingtip Mn(1,4,5,8) are not parallel and at various angles to the plane of the molecule. O31 is on the JT axes of both Mn1 and Mn3, while in the other $Mn_4$ unit O34 is on the JT axes of both Mn6 and Mn8; O31 and O34 are the monoatomically bridging atoms of benzoate groups.

One $Mn_4$ unit of **4** is shown in Figure 3, including its two $\mu_3$-$O^{2-}$ ions and the $Me_2AsO_2^-$ and $PhCO_2^-$ groups providing

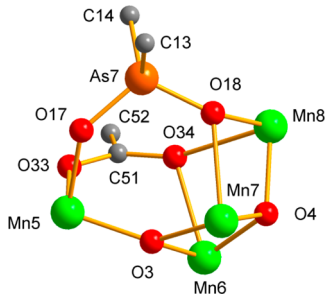


**Figure 3.** Representative example of the $Mn_4$ units in **4** and **5** showing the asymmetric butterfly topology resulting from the location of monatomic bridging O atoms of $PhCO_2^-$ and $Me_2AsO_2^-$ groups. Color code: $Mn^{III}$ green, As orange, O red, C gray.

additional monatomic bridges. The latter are both on the same side and cause a distinct asymmetry not seen in the common symmetric butterfly complexes, such as $[Mn^{III}_4O_2(O_2CR)_7(bpy)_2]^+$,[46] and which is reflected in, for example, shorter $Mn_b\cdots Mn_w$ separations and smaller $Mn_w$–$O_{ox}$–$Mn_b$ angles for the bis-monoatomically bridged $Mn_2$ pairs (Table 5). The resulting $Mn_4$ structure is clearly related to the $\{Mn_4O_4\}$ cubane core of **3**; replacement of the $Me_2AsO_2^-$ and $PhCO_2^-$ groups with $O^{2-}$ ions at the O18 and O34 positions, and attachment to Mn5 by tilting of the Mn5–O3 bond, would give a $\{Mn^{III}_4O_4\}$ cubane. Of course, **3** has a $\{Mn^{IV}_2Mn^{III}_2O_4\}$ cubane, stabilizing the higher $O^{2-}$/Mn ratio of 1:1 and rationalizing why the $Mn^{III}_4$ units in **4** and **5** favor incorporation of only two $O^{2-}$ ions.

There are a remarkable number of different binding modes adopted by the organic groups in **4** and **5**, and these are shown in Figure 4. The $Me_2AsO_2^-$ and $PhCO_2^-$ groups range from

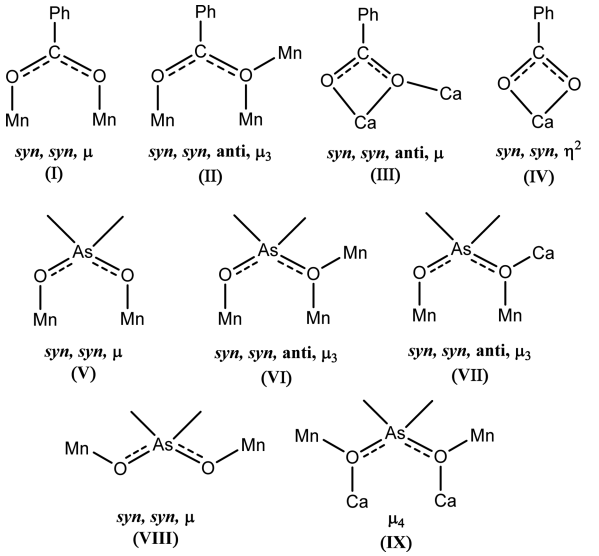


**Figure 4.** Four $PhCO_2^-$ and five $Me_2AsO_2^-$ binding modes in complexes **4** and **5**.

$\mu_2$–$\mu_4$, with various combinations of syn and anti O lone pairs being used for bond formation. The 16 benzoates divide into four each of types I–IV, and the 24 dimethylarsinates into eight, four, eight, two, and two of types V–IX, respectively.

Finally, there are only insignificant intermolecular interactions between $Mn_{16}$ molecules, mostly C–H···C contacts, but no $\pi$–$\pi$ stacking of benzoate rings. It is thus anticipated that any intermolecular exchange interactions would be very weak.

**Magnetochemistry. Direct-Current Magnetic Susceptibility Studies.** Solid-state, variable-temperature magnetic susceptibility ($\chi_M$) data were collected on vacuum-dried microcrystalline samples of complexes **3**·$H_2O$, **4**·2MeCN, and **5** in the 5.0–300 K range in a 0.1 T (1000 G) dc magnetic field. The samples were suspended in eicosane to prevent torquing.

For **3**·$H_2O$, $\chi_MT$ decreases steadily with decreasing $T$ from 8.4 $cm^3$ K $mol^{-1}$ at 300 K to 4.6 $cm^3$ K $mol^{-1}$ at 15 K, and then steeply increases to 5.7 $cm^3$ K $mol^{-1}$ at 5.0 K (Figure 5). The spin-only ($g$ = 2) $\chi_MT$ for noninteracting $Mn^{III}_2Mn^{IV}_2$ ions is 9.75 $cm^3$ K $mol^{-1}$, and thus **3**·$H_2O$ clearly contains dominant antiferromagnetic (AF) intramolecular exchange interactions, although the origin of the increase below 5.0 K was not immediately obvious.



DOI: 10.1021/acs.inorgchem.6b01077
Inorg. Chem. 2016, 55, 8468–8477

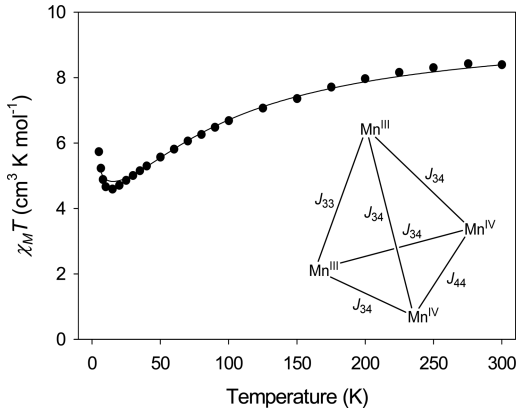


**Figure 5.** $\chi_M T$ vs $T$ plot for **3**·$H_2O$ in a 1000 G dc field. The solid line is the fit of the data using the 3-$J$ model shown in the inset. See the text for the spin Hamiltonian and the fit parameters.

The isotropic Heisenberg spin Hamiltonian describing an exchange-coupled $Mn^{III}_2Mn^{IV}_2$ complex such as **3** is given by eq 1, where $J_{33} = J(Mn^{III}Mn^{III})$, $J_{34} = J(Mn^{III}Mn^{IV})$, $J_{44} = J(Mn^{IV}Mn^{IV})$, and $S_i$ ($i$ = 1−4) is the spin of metal $M_i$, using the numbering scheme of Figure 1, with $S_1 = S_3 = {}^3/_2$ and $S_2 = S_4 = 2$; it is assumed from the virtual $D_2$ symmetry that all $Mn^{III}Mn^{IV}$ interactions are equivalent.

$$\mathcal{H} = -2J_{33}(\hat{S}_2\cdot\hat{S}_4) - 2J_{44}(\hat{S}_1\cdot\hat{S}_3) - 2J_{34}(\hat{S}_1\cdot\hat{S}_2 + \hat{S}_1\cdot\hat{S}_4 + \hat{S}_2\cdot\hat{S}_3 + \hat{S}_3\cdot\hat{S}_4) \quad (1)$$

Using an equivalent operator approach based on the Kambe vector coupling method[47] and the coupling scheme $\hat{S}_A = \hat{S}_1 + \hat{S}_3$, $\hat{S}_B = \hat{S}_2 + \hat{S}_4$, and $\hat{S}_T = \hat{S}_A + \hat{S}_B$, the Hamiltonian of eq 1 can be written in the equivalent form of eq 2, and the energy ($E$) of each molecular $S_T$ state is then given by the eigenvalue expression of eq 3, where constant terms $[S_i(S_i + 1)]$ were omitted. The overall multiplicity is 400, made of 60 individual $S_T$ states with values in the $S_T$ = 0−7 range.

$$\mathcal{H} = -J_{33}[S_B^2 - S_2^2 - S_4^2] - J_{44}[S_A^2 - S_1^2 - S_3^2] - J_{34}[S_T^2 - S_A^2 - S_B^2] \quad (2)$$

$$E(S_T, S_A, S_B) = -J_{33}[S_B(S_B + 1)] - J_{44}[S_A(S_A + 1)] - J_{34}[S_T(S_T + 1) - S_A(S_A + 1) - S_B(S_B + 1)] \quad (3)$$

The data were fit to the theoretical $\chi_M$ versus $T$ expression derived from the use of the Van Vleck equation,[48] including a temperature-independent paramagnetism term kept constant at 400 × $10^{-6}$ cm$^3$ K mol$^{-1}$. The fit (solid line in Figure 5) gave $J_{33}$ = 0.0(1) cm$^{-1}$, $J_{34}$ = −3.4(4) cm$^{-1}$, $J_{44}$ = −9.8(2) cm$^{-1}$, and $g$ = 1.99(1). $J_{34}$ and $J_{44}$ being AF is as expected for bis-$O^{2-}$ bridged $Mn^{III}Mn^{IV}$ and $Mn^{IV}Mn^{IV}$ interactions. However, they are weaker than expected for dinuclear $[Mn_2(\mu\text{-}O^{2-})_2]^{3+,4+}$ compounds, which can be rationalized by their incorporation into an $Mn_4$ cubane and the $O^{2-}$ ions becoming $\mu_3$. For example, the latter makes the $Mn^{IV}\cdots Mn^{IV}$ separation (2.8857(8) Å), $Mn^{IV}-O_c-Mn^{IV}$ angles (97.11(12), 97.69(11)°), and $Mn^{IV}-O^{2-}$ lengths (1.874(3)−1.959(3) Å) significantly larger than those in dinuclear $[Mn^{IV}_2(\mu\text{-}O^{2-})_2]^{4+}$ complexes, 2.58−2.67 Å, 91.6−94.5°, and 1.79−1.81 Å, respectively, which will weaken the interactions.[49] Nevertheless, the $|J_{44}| > |J_{34}| > |J_{33}|$ order is as expected, and the following explanation of the $\chi_M T$ versus $T$ plot (Figure 5) can be given: $\chi_M T$ decreases with decreasing $T$ due to the AF $J_{44}$ and $J_{34}$, and eventually the stronger $J_{44}$ pairs up the $Mn^{IV}_2$ spins into a diamagnetic $S_A$ = 0 state. $J_{34}$ is now nullified, and the only interaction affecting the $Mn^{III}$ spins is thus $J_{33}$, which is zero or essentially so. The $\chi_M T$ for two noninteracting $Mn^{III}$ is 6.0 cm$^3$ K mol$^{-1}$ or slightly less, since $g$ < 2.0 for $Mn^{III}$. This explains the small increase in $\chi_M T$ to 5.7 cm$^3$ K mol$^{-1}$ at 5.0 K, as the two $Mn^{IV}$ spins align antiparallel, and the two $Mn^{III}$ are the only contributors to $\chi_M T$. Note that $J_{33} \approx 0$ is consistent with the alignment of the JT axes parallel and in the $Mn^{III}_2(\mu\text{-}O^{2-})_2$ plane: there will be overlap of the $d_{z^2}$ magnetic orbital of one $Mn^{III}$ with the empty $d_{x^2-y^2}$ of the other, giving a weak ferromagnetic (F) contribution to $J_{33}$ according to standard Goodenough−Kanamori rules,[50] which in this case is clearly of comparable magnitude to the weak AF contributions expected from $d_\pi - d_\pi$ overlap via the $O^{2-}$ orbitals.

For **4**·2MeCN and **5**, $\chi_M T$ decreases with decreasing $T$ from, respectively, 43.9 and 42.9 cm$^3$ K mol$^{-1}$ at 300 K to 16.7 and 15.8 cm$^3$ K mol$^{-1}$ at 5.0 K (Figure 6). The plot profiles and the

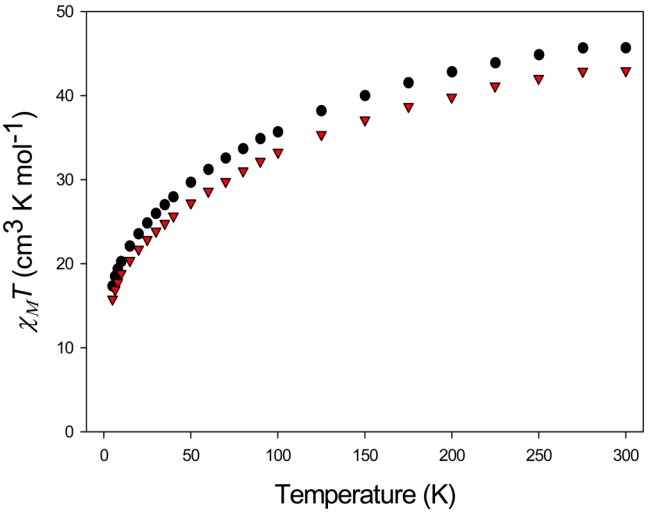


**Figure 6.** $\chi_M T$ vs $T$ plots for **4**·2MeCN (red) and **5** (black) in a 1000 G dc field.

$\chi_M T$ at 300 K being less than the spin-only value for 16 noninteracting $Mn^{III}$ (48 cm$^3$ K mol$^{-1}$ with $g$ = 2) indicate dominant AF exchange interactions. An important question in analyzing further the magnetic properties of **4** and **5** was whether they should be treated as one $Mn_{16}$ unit or as a tetramer of four weakly interacting $Mn_4$ units. Of course, the pertinent point was whether the intra-$Mn_4$ interactions were significantly stronger than inter-$Mn_4$ ones. The inter-$Mn_4$ interactions through the $Me_2AsO_2^-$ groups (Figure 4, types VIII and IX) are certainly expected to be weak, but so should be many of the intra-$Mn_4$ ones, since, as described, it has structural similarity to the core of **3**, and its $[Mn^{III}_2(\mu\text{-}O)_2]$ interactions will likely be similar to those in the latter, which are $J_{33} \approx 0$ cm$^{-1}$. Even symmetric butterflies such as the $[Mn^{III}_4O_2(O_2CR)_7(L\text{-}L)_2]^{0,+}$ family with only one monoatomically bridging oxo are known to have very weak $J_{wb}$, typically in the −3 to −8 cm$^{-1}$ range.[44] We thus concluded that **4** and **5** could be reasonably considered as either single $Mn_{16}$ clusters or looplike tetramers of $Mn_4$ units.

In either case, attempts to determine the ground states from fits using program MAGNET[51] of magnetization ($M$) data collected in the 0.10−70 kG and 1.8−10.0 K ranges were unsuccessful, even using only data at lower fields and $T$ (0.1−0.5 T and 1.8−4.0 K), as anticipated from the many expected


DOI: 10.1021/acs.inorgchem.6b01077
Inorg. Chem. 2016, 55, 8468−8477

weak $J_{ij}$ and the resulting low-lying excited states. Also, depending on relative $J_{ij}$ sign and magnitude, there may be spin frustration effects in the triangular $Mn_3$ subunits of each $Mn_4$, which are also known to promote low-lying excited states; spin frustration is here defined in the form most useful to molecular chemistry, that is, competing exchange interactions of comparable magnitude that frustrate the preferred alignments of the spins. In such cases, a more reliable way to get information on ground-state spins is by ac magnetic susceptibility, which precludes complications from a dc field.

**Alternating Current Magnetic Susceptibility Studies.** The ac magnetic susceptibility data were collected on dried, microcrystalline samples in the 1.8−10 K range in zero dc field and a 3.5 G ac field at oscillation frequencies in the 25−1000 Hz range. For **4**·2MeCN considered as a single $Mn_{16}$ unit, the in-phase $\chi'_M T$ decreases almost linearly from ∼13 $cm^3$ K $mol^{-1}$ at 10 K to ∼10 $cm^3$ K $mol^{-1}$ at 3 K, and then decreases a little faster at lower $T$ (Figure 7) probably due to zero-field splitting

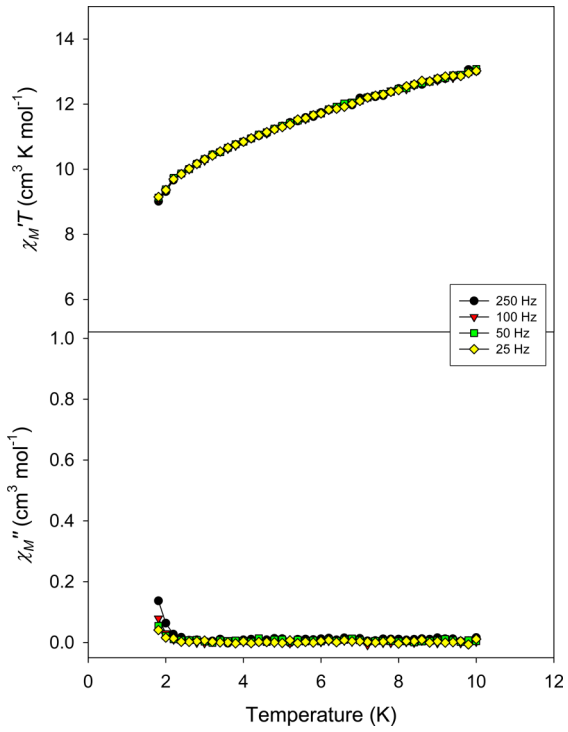


**Figure 7.** $\chi'_M T$ vs $T$ and $\chi''_M$ vs $T$ ac susceptibility plots for **4**·MeCN at the indicated frequencies. The solid lines are guides.

and weak intermolecular interactions. The decrease below 10 K indicates depopulation of low-lying excited states with spin greater than the ground state and rationalizes the unsuccessful attempts at fitting the dc data. Extrapolation of the $\chi'_M T$ above 3 to 0 K, where only the ground state will be populated, gives a value slightly below 10 $cm^3$ K $mol^{-1}$, consistent with an $S = 4$ ground state with $g < 2$ slightly, as expected for $Mn^{III}$; $\chi'_M T$ for $S = 3$, 4, and 5 spins with $g = 2.0$ are 6.0, 10.0, and 15.0 $cm^3$ K $mol^{-1}$, respectively. Complex **5** exhibits almost identical $\chi'_M T$ data (Figure S2).

If the data are interpreted taking **4** as a $[Mn_4]_4$ tetramer of very weakly interacting units, $\chi'_M T$ per $Mn_4$ decreases almost linearly from ∼3.25 $cm^3$ K $mol^{-1}$ at 10 K to ∼2.5 $cm^3$ K $mol^{-1}$ at 3 K. The faster decrease below 3 K can now be assigned to inter-$Mn_4$ interactions in addition to any intermolecular interactions. The extrapolation to 0 K now gives a value of ∼2.4 $cm^3$ K $mol^{-1}$, indicative of an $S = 2$ ground state and $g < 2$ for each $Mn_4$ unit ($\chi'_M T$ for $S = 1$, 2, and 3 with $g = 2.0$ are 1.0, 3.0, and 6.0 $cm^3$ K $mol^{-1}$, respectively). Similarly for **5**.

Interestingly, both complexes exhibit very weak out-of-phase $\chi''_M$ signals below 3 K, possibly the beginnings of peaks lying far below the operating limit of 1.8 K of our instrument, suggesting that they may both be SMMs, albeit very poor ones with clearly small relaxation energy barriers. Nevertheless, since they would be our first with these arsinate ligands, we sought to confirm this by hysteresis studies below 1.8 K.

**Hysteresis Measurements.** Magnetization versus dc field sweeps below 1.8 K were performed on a wet crystal of **4**·15MeCN freshly removed from its mother liquor. Hysteretic behavior was observed, but with unusual characteristics (Figure 8). The loops at 0.04 K at different scan rates show a small

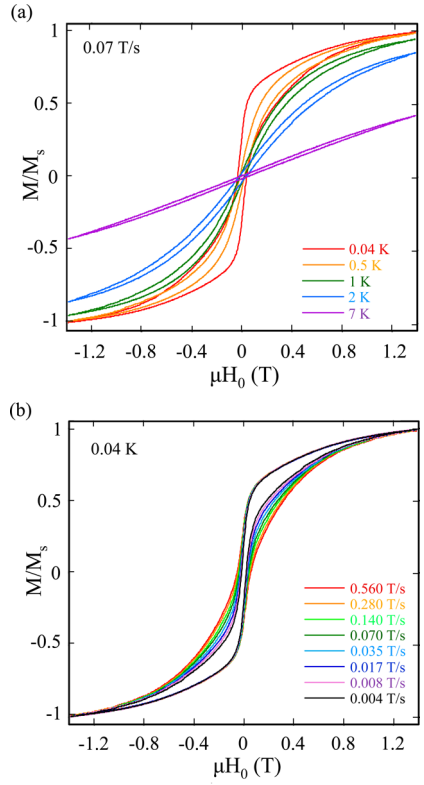


**Figure 8.** $M$ vs $\mu_0 H$ (in tesla) hysteresis loops for a single crystal of **4**·15MeCN at (a) the indicated temperatures and a fixed field sweep rate of 0.07 T/s and (b) the indicated field sweep rates and a fixed temperature of 0.04 K. The magnetization is normalized to its saturation value ($M_S$).

coercivity, which increases with the scan rate as expected for an SMM, but not by much. In addition, the $T$-dependence at a fixed scan rate (Figure 8a) exhibits decreasing coercivity with $T$, as also expected for an SMM, with a hysteretic opening even at 7 K. This is surprising, since **4** and **5** clearly do not have large enough anisotropy barriers to make them such relatively high-temperature SMMs. Overall, the loops for **4** are not typical of those expected for an SMM, and we instead must conclude that the observed behavior is coming from a combination of effects, such as a small anisotropy barrier intrinsic to each magnetic unit, interunit interactions, perhaps phonon bottlenecks, and others. Since the crystal structure shows no significant inter-$Mn_{16}$ contacts (vide supra), we feel the hysteresis loops support


DOI: 10.1021/acs.inorgchem.6b01077
Inorg. Chem. 2016, 55, 8468−8477

**4** and **5** being best described magnetically as loops of four $Mn_4$ units, with inter-$Mn_4$ exchange interactions through the bridging $Me_2AsO_2^-$ groups in modes VIII and IX (Figure 4) contributing to the unusual hysteresis behavior. Note that this would also explain the clear slope of the background in Figure 8, which suggests the applied field is not along the easy axes of all magnetic units, as would be expected if each $Mn_{16}$ is really four $Mn_4$ units with nonequivalent orientations in the molecule.

It is interesting to note that analogous behavior has been previously seen in the hysteresis studies for a looplike $[Mn_{10}Na]_4$ tetramer, that is, a sloping background and a coercivity that varies only slightly with scan rate and is still visible up to 4 K, even though the intrinsic anisotropy barrier for each $Mn_{10}$ unit is small. That this compound and **4** are both tetramers of four weakly interacting magnetic units may just be a coincidence or maybe not. Further studies are necessary to address this point.

## CONCLUSIONS

The use of $Me_2AsO_2H$ in Mn cluster chemistry has yielded initial examples of Mn clusters ligated by $Me_2AsO_2^-$ groups, and they have been found to be interesting from multiple viewpoints. Attempted ligand substitution on $[Mn_{12}O_{12}(O_2CMe)_{16}(H_2O)_4]$ has led to structural transformation to cubane **3**, obtained in large yield. The behavior of the As acid has thus paralleled that of its group 16 neighbor Se to its right in causing structural rearrangement—but it does not yield analogous products; on the contrary, it has given a cubane, as has been obtained previously with its group 15 neighbor P. As discussed above, we assign the analogous behavior of As and Se as due to the increased size and lowered electronegativity of the central atom, which gives relatively large O···O distances and high basicity to the ligands, as reflected in the p$K_a$ values of the conjugate acids, particularly for As. The heterometallic chemistry of $Me_2AsO_2H$ has also yielded interesting products, looplike clusters **4** and **5** that are unusual in both their structures and magnetic properties. One conclusion of possible general utility is that the occasional observation of small coercivity at relatively high $T$, in this case 7 K, that fades only slowly with $T$, does not necessarily represent an improved SMM.

Together with the unusual magnetic behavior of cubane **3**, the combined results suggest that $Me_2AsO_2H$ has the potential to continue to provide further compounds that will be of interest for their structural and/or magnetic properties. Further studies are thus in progress.

## ASSOCIATED CONTENT

### Supporting Information

The Supporting Information is available free of charge on the ACS Publications website at DOI: 10.1021/acs.inorgchem.6b01077.

X-ray crystallographic data in CIF format for complexes **3**–**5** (CIF)

Error surface plots of $D$ versus $g$, magnetic susceptibility plots versus temperature, and extended tables of selected bond distances and angles. (PDF)

## AUTHOR INFORMATION

### Corresponding Author

*E-mail: christou@chem.ufl.edu. Phone: +1-352-392-8314. Fax: +1-352-392-8757.

### Notes

The authors declare no competing financial interest.

## ACKNOWLEDGMENTS

We thank the National Science Foundation (Grant No. DMR-1213030) for support of this work.

## REFERENCES

(1) (a) Christou, G.; Gatteschi, D.; Hendrickson, D. N.; Sessoli, R. *MRS Bull.* **2000**, *25*, 66–71. (b) Gatteschi, D.; Sessoli, R. *Angew. Chem., Int. Ed.* **2003**, *42*, 268–297. (c) Sessoli, R.; Tsai, H.-L.; Schake, A. R.; Wang, S.; Vincent, J. B.; Folting, K.; Gatteschi, D.; Christou, G.; Hendrickson, D. N. *J. Am. Chem. Soc.* **1993**, *115*, 1804. (d) Sessoli, R.; Gatteschi, D.; Caneschi, A.; Novak, M. A. *Nature* **1993**, *365*, 141.

(2) (a) Christou, G. *Polyhedron* **2005**, *24*, 2065–2075. (b) Bagai, R.; Christou, G. *Chem. Soc. Rev.* **2009**, *38*, 1011–1026.

(3) (a) Rinehart, J. D.; Fang, M.; Evans, W. J.; Long, J. R. *Nat. Chem.* **2011**, *3*, 538–542. (b) Rinehart, J. D.; Fang, M.; Evans, W. J.; Long, J. R. *J. Am. Chem. Soc.* **2011**, *133*, 14236–14239.

(4) Woodruff, D. N.; Winpenny, R. E.; Layfield, R. A. *Chem. Rev.* **2013**, *113*, 5110–5148.

(5) Aromi, G.; Brechin, E. K. *Struct. Bonding (Berlin)* **2006**, *122*, 1–67.

(6) Craig, G. A.; Murrie, M. *Chem. Soc. Rev.* **2015**, *44*, 2135–2147.

(7) (a) Pereira, L. C. J.; Camp, C.; Coutinho, J. T.; Chatelain, L.; Maldivi, P.; Almeida, M.; Mazzanti, M. *Inorg. Chem.* **2014**, *53*, 11809–11811. (b) Moro, F.; Mills, D. P.; Liddle, S. T.; van Slageren, J. *Angew. Chem., Int. Ed.* **2013**, *52*, 3430–3433.

(8) (a) Osa, S.; Kido, T.; Matsumoto, N.; Re, N.; Pochaba, A.; Mrozinski, J. *J. Am. Chem. Soc.* **2004**, *126*, 420–421. (b) Zaleski, C. M.; Depperman, E. C.; Kampf, J. W.; Kirk, M.-L.; Pecoraro, V. L. *Angew. Chem., Int. Ed.* **2004**, *43*, 3912–3914. (c) Mishra, A.; Wernsdorfer, W.; Abboud, K. A.; Christou, G. *J. Am. Chem. Soc.* **2004**, *126*, 15648–15649. (d) Stamatatos, T. C.; Teat, S. J.; Wernsdorfer, W.; Christou, G. *Angew. Chem., Int. Ed.* **2009**, *48*, 521–524.

(9) (a) Mereacre, V.; Ako, A. M.; Clerac, R.; Wernsdorfer, W.; Filoti, G.; Bartolome, J.; Anson, C. E.; Powell, A. *J. Am. Chem. Soc.* **2007**, *129*, 9248–9249. (b) Mereacre, V.; Ako, A. M.; Clerac, R.; Wernsdorfer, W.; Hewitt, I. J.; Anson, C. E.; Powell, A. K. *Chem.–Eur. J.* **2008**, *14*, 3577–3584. (c) Langley, S.; Moubaraki, B.; Murray, K. S. *Dalton Trans.* **2010**, *39*, 5066–5069. (d) Karotsis, G.; Kennedy, S.; Teat, S. J.; Beavers, C. M.; Fowler, D. A.; Morales, J. J.; Evangelisti, M.; Dalgarno, S. J.; Brechin, E. K. *J. Am. Chem. Soc.* **2010**, *132*, 12983–12990. (e) Mereacre, V.; Lan, Y.; Clerac, R.; Ako, A. M.; Hewitt, I. J.; Wernsdorfer, W.; Buth, G.; Anson, C. E.; Powell, A. K. *Inorg. Chem.* **2010**, *49*, 5293–5302. (f) Liu, C.-M.; Zhang, D.-Q.; Zhu, D.-B. *Dalton Trans.* **2010**, *39*, 11325–11328.

(10) (a) Papatriantafyllopoulou, C.; Wernsdorfer, W.; Abboud, K. A.; Christou, G. *Inorg. Chem.* **2011**, *50*, 421–423. (b) Holyńska, M.; Premuzič; Jeon, I.- R.; Wernsdorfer, W.; Clerac, R.; Dehnen, S. *Chem.–Eur. J.* **2011**, *17*, 9605–9610.

(11) Rosado Piquer, L.; Sanudo, E. C. *Dalton Trans.* **2015**, *44*, 8771–8780.

(12) (a) Tasiopoulos, A. J.; Vinslava, A.; Wernsdorfer, W.; Abboud, K. A.; Christou, G. *Angew. Chem., Int. Ed.* **2004**, *43*, 2117. (b) Vinslava, A.; Tasiopoulos, A. J.; Wernsdorfer, W.; Abboud, K. A.; Christou, G. *Inorg. Chem.* **2016**, in press. DOI: 10.1021/acs.inorgchem.5b02790.

(13) (a) Eppley, H. J.; Tsai, H.-L.; de Vries, N.; Folting, K.; Christou, G.; Hendrickson, D. N. *J. Am. Chem. Soc.* **1995**, *117*, 301–317. (b) Soler, M.; Wernsdorfer, W.; Abboud, K. A.; Huffman, J. C.; Davidson, E. R.; Hendrickson, D. N.; Christou, G. *J. Am. Chem. Soc.* **2003**, *125*, 3576–3588. (c) Chakov, N. E.; Soler, M.; Wernsdorfer, W.; Abboud, K. A.; Christou, G. *Inorg. Chem.* **2005**, *44*, 5304–5321.

(14) (a) Bian, G.-Q.; Kuroda-Sowa, T.; Gunjima, N.; Maekawa, M.; Munakata, M. *Inorg. Chem. Commun.* **2005**, *8*, 208–211.

(15) (a) Soler, M.; Wernsdorfer, W.; Sun, Z.; Huffman, J. C.; Hendrickson, D. N.; Christou, G. *Chem. Commun.* **2003**, *21*, 2672–2673. (b) Zhao, H.; Berlinguette, C. P.; Bacsa, J.; Prosvirin, A. V.; Bera,



DOI: 10.1021/acs.inorgchem.6b01077
*Inorg. Chem.* 2016, 55, 8468–8477

J. K.; Tichy, S. E.; Schelter, E. J.; Dunbar, K. R. *Inorg. Chem.* **2004**, *43*, 1359−1369.
(16) Soler, M.; Artus, P.; Folting, K.; Huffman, J. C.; Hendrickson, D. N.; Christou, G. *Inorg. Chem.* **2001**, *40*, 4902−4912.
(17) Artus, P.; Boskovic, C.; Yoo, J.; Streib, W. E.; Brunel, L.-C.; Hendrickson, D. N.; Christou, G. *Inorg. Chem.* **2001**, *40*, 4199−4210.
(18) (a) Boskovic, C.; Pink, M.; Huffman, J. C.; Hendrickson, D. N.; Christou, G. *J. Am. Chem. Soc.* **2001**, *123*, 9914−9915. (b) Brockman, J. T.; Abboud, K. A.; Hendrickson, D. N.; Christou, G. *Polyhedron* **2003**, *22*, 1765−1769.
(19) (a) Bian, G.-Q.; Kuroda-Sowa, T.; Konaka, H.; Hatano, M.; Maekawa, M.; Munakata, M.; Miyasaka, H.; Yamashita, M. *Inorg. Chem.* **2004**, *43*, 4790−4792. (b) Kuroda-Sowa, T.; Fukuda, S.; Miyoshi, S.; Maekawa, M.; Munakata, M.; Miyasaka, H.; Yamashita, M. *Chem. Lett.* **2002**, *31*, 682−683.
(20) (a) Chakov, N. E.; Wernsdorfer, W.; Abboud, K. A.; Hendrickson, D. N.; Christou, G. *Dalton Trans.* **2003**, *11*, 2243−2248. (b) Chakov, N. E.; Abboud, K. A.; Zakharov, L. N.; Rheingold, A. L.; Hendrickson, D. N.; Christou, G. *Polyhedron* **2003**, *22*, 1759−1763.
(21) Kuroda-Sowa, T.; Handa, T.; Kotera, T.; Maekawa, M.; Munakata, M.; Miyasaka, H.; Yamashita, M. *Chem. Lett.* **2004**, *33*, 540−541.
(22) Chakov, N. E.; Wernsdorfer, W.; Abboud, K. A.; Christou, G. *Inorg. Chem.* **2004**, *43*, 5919−5930.
(23) Gresley, N. M.; Griffith, W. P.; Parkin, B. C.; White, A. J. P.; Williams, D. J. *J. Chem. Soc., Dalton Trans.* **1996**, *10*, 2039−2045.
(24) Lis, T. *Acta Crystallogr., Sect. B: Struct. Crystallogr. Cryst. Chem.* **1980**, *36*, 2042−2046.
(25) (a) Sheldrick, G. M. *SHELXTL5;* Bruker-AXS: Madison, WI, 1998. (b) Bruker. *SAINT*, 6.36a; Bruker AXS, Inc: Madison, WI, 1998. (c) Blessing, R. H. *Acta Crystallogr., Sect. A: Found. Crystallogr.* **1995**, *51*, 33−38.
(26) van der Sluis, P.; Spek, A. L. *Acta Crystallogr., Sect. A: Found. Crystallogr.* **1990**, *46*, 194−201.
(27) Spek, A. L. *Acta Crystallogr.* **1990**, *A46*, 1−11.
(28) Davidson, E. R. *Magnet;* Indiana University: Bloomington, IN, 1999.
(29) Weast, R. C. *CRC Handbook of Chemistry and Physics*; CRC Press, Inc.: Boca Raton, FL, 1984.
(30) *Dissociation Constants of Organic Acids in Aqueous Solution;* Kortüm, G., Vogel, W., Andrussow, K., Eds.; Butterworth: London, U.K, 1961.
(31) See Supporting Information.
(32) (a) Brown, I. D.; Altermatt, D. *Acta Crystallogr., Sect. B: Struct. Sci.* **1985**, *41*, 244−247. (b) Palenik, G. J. *Inorg. Chem.* **1997**, *36*, 4888−4890. (c) Palenik, G. J. *Inorg. Chem.* **1997**, *36*, 122−124.
(33) Kennedy, B. J.; Murray, K. S. *Inorg. Chem.* **1985**, *24*, 1552−1557.
(34) Sun, Z.; Ruiz, D.; Dilley, N. R.; Soler, M.; Ribas, J.; Folting, K.; Maple, M. B.; Christou, G.; Hendrickson, D. N. *Chem. Commun.* **1999**, 1973−1974.
(35) (a) Eulering, B.; Ahlers, F.; Zippel, F.; Schmidt, M.; Nolting, H.-F.; Krebs, B. *J. Chem. Soc., Chem. Commun.* **1995**, *12*, 1305−1307. (b) Eulering, B.; Schmidt, M.; Pinkernell, U.; Karst, U.; Krebs, B. *Angew. Chem., Int. Ed. Engl.* **1996**, *35*, 1973−1974. (c) Than, R.; Schrodt, A.; Westerheide, L.; van Eldik, R.; Krebs, B. *Eur. J. Inorg. Chem.* **1999**, *1999*, 1537−1543. (d) Frisch, J. R.; Vu, V. V.; Martinho, M.; Munck, E.; Que, L. *Inorg. Chem.* **2009**, *48*, 8325−8336.
(36) Albedyhl, S.; Schnieders, D.; Jancso, A.; Gajda, T.; Krebs, B. *Eur. J. Inorg. Chem.* **2002**, *2002*, 1400−1409.
(37) Kumara Swamy, K. C.; Veith, M.; Huch, V.; Mathur, S. *Inorg. Chem.* **2003**, *42*, 5837−5843.
(38) Gresley, N. M.; Griffith, W. P.; Parkin, B. C.; White, A. J. P.; Williams, D. J. *J. Chem. Soc., Dalton Trans.* **1996**, *10*, 2039−2045.
(39) (a) Barkigia, K. M.; Rajković, L. M.; Pope, M. T.; Quicksall, C. O. *J. Am. Chem. Soc.* **1975**, *97*, 4146−4147. (b) Barkigia, K. M.; Rajković-Blazer, L. M.; Pope, M. T.; Prince, E.; Quicksall, C. O. *Inorg. Chem.* **1980**, *19*, 2531−2537. (c) Matsumoto, K. Y. *Bull. Chem. Soc. Jpn.* **1979**, *52*, 3284−3285. (d) Gresley, N. M.; Griffith, W. P.; White, A. J. P.; Williams, D. J. *J. Chem. Soc., Dalton Trans.* **1997**, *1*, 89−92.
(40) Chimamkpam, T. O.; Clérac, R. C.; Mitcov, D.; Twamley, B.; Venkatesan, M.; Schmitt, W. *Dalton Trans.* **2016**, *45*, 1349−1353.
(41) (a) Ruettinger, W. F.; Campana, C.; Dismukes, G. C. *J. Am. Chem. Soc.* **1997**, *119*, 6670−6671. (b) Wu, J.-Z.; Sellitto, E.; Yap, G. P. A.; Sheats, J.; Dismukes, G. C. *Inorg. Chem.* **2004**, *43*, 5795−5797.
(42) Ruettinger, W. F.; Ho, D. M.; Dismukes, G. C. *Inorg. Chem.* **1999**, *38*, 1036−1037.
(43) Hendrickson, D. N.; Christou, G.; Schmitt, E. A.; Libby, E.; Bashkin, J. S.; Wang, S.; Tsai, H.-L.; Vincent, J. B.; Boyd, P. D. W. *J. Am. Chem. Soc.* **1992**, *114*, 2455−2471.
(44) (a) Wemple, M. W.; Adams, D. M.; Folting, K.; Hendrickson, D. N.; Christou, G. *J. Am. Chem. Soc.* **1995**, *117*, 7275−7276. (b) Wemple, M. W.; Adams, D. M.; Hagen, K. S.; Folting, K.; Hendrickson, D. N.; Christou, G. *J. Chem. Soc., Chem. Commun.* **1995**, *15*, 1591−1593. (c) Wang, S.; Folting, K.; Streib, W. E.; Schmitt, E. A.; McCusker, J. K.; Hendrickson, D. N.; Christou, G. *Angew. Chem., Int. Ed. Engl.* **1991**, *30*, 305−306. (d) Wang, S.; Tsai, H.-L.; Libby, E.; Folting, K.; Streib, W. E.; Hendrickson, D. N.; Christou, G. *Inorg. Chem.* **1996**, *35*, 7578−7589.
(45) See Supporting Information.
(46) Vincent, J. B.; Christmas, C.; Chang, H.-R.; Li, Q.; Boyd, P. D. W.; Huffman, J. C.; Hendrickson, D. N.; Christou, G. *J. Am. Chem. Soc.* **1989**, *111*, 2086−2088.
(47) Kambe, K. *J. Phys. Soc. Jpn.* **1950**, *5*, 48−51.
(48) (a) O'Connor, C. *J. Prog. Inorg. Chem.* **1982**, *29*, 203−283. (b) *The Theory of Electric and Magnetic Susceptibilities;* Van Vleck, J. H., Ed.; Oxford University Press: London, U.K, 1932.
(49) Bhaduri, S.; Tasiopoulos, A. J.; Bolcar, M. A.; Abboud, K. A.; Streib, W. E.; Christou, G. *Inorg. Chem.* **2003**, *42*, 1483−1492.
(50) (a) Goodenough, J. B. *Phys. Rev.* **1955**, *100*, 564−573. (b) Goodenough, J. B. *Magnetism and the Chemical Bond;* Interscience: New York, 1963. (c) Kanamori, J. *J. Phys. Chem. Solids* **1959**, *10*, 87. (d) Gingsberg, A. P. *Inorg. Chim. Acta, Rev.* **1971**, *5*, 45.
(51) Davidson, E. R. *Magnet;* Indiana University: Bloomington, IN.
(52) *Handbook of Physical Properties of Organic Chemicals;* Howard, P. H., Meylan, W. M., Eds.; CRC Press: New York, 1997.
(53) McCullough, J.; Gould, E. S. J. *J. Am. Chem. Soc.* **1949**, *71*, 674−676.
(54) *Dissociation Constants of Organic Acids in Aqueous Solution;* Kortüm, G., Vogel, W., Andrussow, K., Eds.; Butterworth: London, U.K, 1961.
(55) Serjean, E. P.; Dempsey, B. *Ionisation Constants of Organic Acids in Aqueous Solution;* Pergamon Press: New York, 1979.


DOI: 10.1021/acs.inorgchem.6b01077
*Inorg. Chem.* 2016, 55, 8468−8477